Chemotaxis and autochemotaxis of self-propelling droplet swimmers

Chenyu Jin[a], Carsten Krüger[a], and Corinna C. Maass[a,1]

[a]Department Dynamics of Complex Fluids, Max Planck Institute for Dynamics and Self-Organization, Am Fassberg 17, 37077 Goettingen, Germany

Edited by Tom C. Lubensky, University of Pennsylvania, Philadelphia, PA, and approved April 6, 2017 (received for review December 6, 2016)

Chemotaxis and autochemotaxis play an important role in many essential biological processes. We present a self-propelling artificial swimmer system that exhibits chemotaxis as well as negative autochemotaxis. Oil droplets in an aqueous surfactant solution are driven by interfacial Marangoni flows induced by micellar solubilization of the oil phase. We demonstrate that chemotaxis along micellar surfactant gradients can guide these swimmers through a microfluidic maze. Similarly, a depletion of empty micelles in the wake of a droplet swimmer causes negative autochemotaxis and thereby trail avoidance. We studied autochemotaxis quantitatively in a microfluidic device of bifurcating channels: Branch choices of consecutive swimmers are anticorrelated, an effect decaying over time due to trail dispersion. We modeled this process by a simple one-dimensional diffusion process and stochastic Langevin dynamics. Our results are consistent with a linear surfactant gradient force and diffusion constants appropriate for micellar diffusion and provide a measure of autochemotactic feedback strength vs. stochastic forces. This assay is readily adaptable for quantitative studies of both artificial and biological autochemotactic systems.

artificial swimmers | chemotaxis | autochemotaxis | microfluidics

Locomotion of living bacteria or cells can be random or oriented. Oriented motion comprises the various "taxis" strategies by which bacteria or cells react to changes in their environment (1). Among these, chemotaxis is one of the best-studied examples (2, 3): Cells and microorganisms are able to sense certain chemicals (chemoattractants or chemorepellents) and move toward or away from them. This is an essential function in many biological processes, e.g., wound healing, fertilization, pathogenic species invading a host, or colonization dynamics (4, 5). When the chemoattractant or chemorepellent is produced by the microorganisms themselves, the system exhibits positive or negative autochemotaxis. Thus, chemotaxis provides a mechanism of interindividual communication. Modeling such communication strategies is key to understanding the collective behavior of microorganisms (6–8) as well as flocks of animals like fire ants (9, 10).

To model the swimming motion of microorganisms, various self-propelling artificial swimmer systems have been developed based on different mechanisms. Generally, there are two classes of swimmers: systems driven by and aligning with external fields (11–14), including chemotactic gradients, and self-propelled swimmers, which move autonomously in homogeneous environments (15–21). Many autonomous swimmers additionally react to external fields, e.g., phototactic gradients (22).

Biological autochemotactic systems exhibit very complex behaviors (23, 24), where physical effects are intermingling with effects from various bioprocesses such as cell migration, metabolism, and division. To untangle these effects, there have been some design proposals for artificial systems, such as in ref. 25, and simulations on the dynamics of simple autochemotactic microswimmers (26–30). Studies exist on collective effects like autochemotaxis-induced clustering (31–33), but generally, there is still a lack of well-controllable and quantifiable experimental realizations of autochemotactic artificial swimmers. We demonstrate chemotaxis and autochemotaxis in microfluidic geometries for a highly symmetric and tunable artificial model swimmer system: self-propelling oil droplets in an aqueous surfactant solution (15, 34, 35).

The quantitative study of chemotaxis with traditional methods such as micropipette assays has been limited to observational studies (36, 37), as experimental conditions such as gradient strength are difficult to set in such geometries. Using microfluidic techniques, experimental conditions can be much better controlled; e.g., a linear gradient can be generated and kept constant, or even fast switched (38, 39), the object distribution can be easily analyzed (40), and the objects can be tracked individually (41–43). In this paper we present a microfluidic assay for the quantitative study of autochemotaxis. We have not only observed autochemotaxis reproducibly, but also been able to directly measure system parameters like diffusion constants. This enables further quantitative experimental studies on the dynamics of simple autochemotactic swimmers.

Self-Propelling Droplet Swimmers

When an oil droplet dissolves in a surfactant solution, oil molecules will continuously migrate into the surfactant micelles until the entire droplet is solubilized. The final equilibrium state of the system is a homogeneous micellar nanoemulsion, composed of a mixture of empty micelles, oil-filled micelles, and free surfactant molecules at the critical micelle concentration (CMC). The droplet locomotion is caused by a self-sustained Marangoni flow due to the inhomogeneous interfacial surfactant coverage and only observable in the nonequilibrium state of solubilization (Fig. 1) (35). While incorporating oil molecules, micelles grow in size, incorporating free surfactant molecules from the aqueous phase and increasing the total area of oil–water interfaces in the system. A boundary layer forms around the droplet with a

Significance

Chemotaxis and autochemotaxis are key mechanisms in the dynamics of microorganisms, e.g., in the acquisition of nutrients and in the communication between individuals, as well as influencing their collective behavior. However, chemical signaling and the natural environment of biological swimmers are generally complex, such that control parameters are hard to single out and quantify experimentally. Here, artificial systems with biomimetic features can provide vital insights. We present a well-controllable droplet swimmer system exhibiting both chemotaxis and negative autochemotaxis, as well as microfluidic assays to observe, control, and quantify these effects. Fundamental properties of the system can be derived by a simple analytical model.

Author contributions: C.J. and C.K. designed research; C.J. and C.K. performed research; C.J., C.K., and C.C.M. analyzed data; and C.J. and C.C.M. wrote the paper.

The authors declare no conflict of interest.

This article is a PNAS Direct Submission.

[1]To whom correspondence should be addressed. Email: corinna.maass@ds.mpg.de.

This article contains supporting information online at www.pnas.org/lookup/suppl/doi:10.1073/pnas.1619783114/-/DCSupplemental.

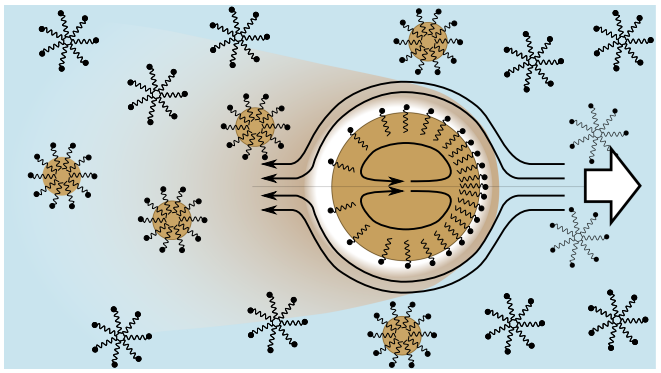

Fig. 1. Schematic drawing of a droplet swimmer moving in surfactant solution. Due to the micellar solubilization of the oil phase, filled micelles disperse from the droplet into the solution, as shown by the yellowish shadow. Close to the droplet the free surfactant molecules are depleted, as shown by the white circle. When the droplet moves, it encounters more empty micelles in the front and leaves more filled micelles behind. The inhomogeneous interfacial surfactant coverage on the droplet then starts the Marangoni flow and sustains the motion. Drawing is not to scale.

reduced density of free surfactant that in turn depletes the surfactant coverage of the droplet interface. This depletion is counteracted by the disintegration of empty micelles approaching the droplet either via diffusion or, if the droplet is moving, via advection. Advection will lead to more available empty micelles in front of the droplet and a trail of filled micelles behind it. In consequence, the depletion at the droplet apex is less pronounced and the resulting Marangoni flow will drive the droplet farther forward toward even more empty micelles. At sufficiently high surfactant concentrations, small fluctuations in the droplet position or surfactant density are sufficient to start sustained self-propulsion. In flow equilibrium, set by the balance of Marangoni forces and viscous dissipation, the swimmer moves at a constant speed controlled by the global surfactant concentration.

The system presented in this study uses the ionic surfactant tetradecyltrimethylammonium bromide (TTAB); the oil phase consists of the nematic liquid crystal 4-pentyl-4'-cyano-biphenyl (5CB). Nematic droplet swimmers of pure 5CB exhibit a strong curling instability (44) in their propulsion, which is absent in isotropic droplets. For this study, we use only isotropic droplets, either by keeping the ambient temperature above the nematic–isotropic transition at $T_{NI} = 35^{\circ}$C or by substituting a mixture of 5CB and 1-Bromopentadecane (BPD) with a volume ratio of 10:1. Henceforth, we refer to the respective droplet types using the notations 5CB and 5CB/BPD. Droplets are mass produced in microfluidic flow-focusing devices with high monodispersity ($<5\%$) and sizes adjustable between 30 μm and 100 μm. The observation time is on the order of hours. Droplet speed and trajectory persistence are well controllable via temperature and surfactant concentration (44). The droplet propulsion is initiated at surfactant concentrations above 4 wt% TTAB.

Chemotactic Maze Solving

Following the argument above, an external gradient of surfactant, i.e., empty micelles, will result in an alignment of the Marangoni flow with the gradient direction; as a result the droplet swimmer will move toward higher surfactant concentrations. This behavior is typical for chemotaxis: The swimmer has no preferred direction in a homogeneous medium, yet moves directionally in the presence of a chemical gradient.

To demonstrate the chemotactic nature of our droplet swimmers, we used a design inspired by Lagzi et al. (11) consisting of two reservoirs connected by a microfluidic maze (Fig. 2). Chemoattractant released at the exit spreads into the maze, with the local concentration depending on the path distance to the exit. By moving up gradients, swimmers will then prefer the shortest path, as shown in chemotactic experimental systems (11, 12) and simulations (45).

To initiate droplet propulsion, the maze is prefilled with a micellar TTAB solution at 5 wt%. Directly after the droplet swimmers (5CB/BPD) are released into the entrance reservoir, solid TTAB is added to the exit reservoir, acting as a chemoattractant. The TTAB gradually dissolves and spreads into the maze via convective diffusion, i.e., significantly faster than simple micellar diffusion. Thus, there will be a positive gradient along the optimum path through the maze, attracting the swimmers, whereas dead ends and detours will feature negative gradients, repelling the swimmers back toward the shortest path. In a control experiment, we prefilled the maze again with a 5 wt% TTAB solution, but added no solids, such that the overall concentration was homogeneous.

Fig. 2 shows results from our experiment. In Fig. 2*A*, we imaged the surfactant spreading inside the maze qualitatively by mixing the solid TTAB with the fluorescent Nile Red dye, which is insoluble in water and therefore comoves with the surfactant micelles. The still image in Fig. 2*A* is taken 60 min after the release of solid TTAB; the additional surfactant has spread to the maze entrance and its concentration decreases along side branches.

Fig. 2 *C* and *D* shows the trajectories of swimmers in a gradient (Fig. 2*C*) and a control experiment (Fig. 2*D*) during a 90-min time interval. The trajectories are color coded by time from blue to red. In the presence of a surfactant gradient, (Fig. 2*C*), the trajectory density is highest along the shortest path, with detours occurring primarily in the first 20 min, before the surfactant has spread sufficiently. In the control experiment without a gradient (Fig. 2*D*), the swimmers move freely and explore the entire maze, with no correlations in time.

Fig. 2*B* compares trajectory lengths between gradient and control experiments for all swimmers that successfully traversed the maze, sorted by the time at which they entered the maze.

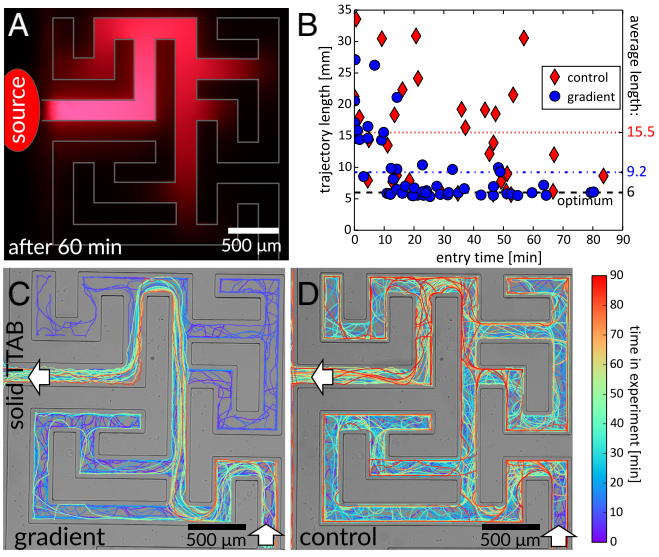

Fig. 2. Maze solving by chemotactic droplet swimmers. White arrows indicate maze entrance and exit. (*A*) Solid TTAB mixed with fluorescent Nile Red spreading in the maze; distribution after 60 min. "Source" marks the point of release (the excitation LED was shaded in this area to improve contrast). (*C* and *D*) Trajectories with and without TTAB gradient. We selected only swimmers that passed both entrance and exit points. Line colors correspond to the time in the experiment. In *C*, detours are mostly for early times (purple) whereas in *D* there is no correlation. (*B*) Plot of path lengths vs. entry time, compared with the shortest path length (6 mm) (Movies S1–S3).

Initially, trajectory lengths are comparable between both experiments. After 20 min, in the presence of a well-established gradient (blue circles), over 80% of the recorded trajectories approach the optimum length of 6 mm, with an average trajectory length of 9.2 mm over the entire duration of the experiment. Without a gradient (red diamonds), the trajectory length is on average (15.5 mm) more than twice the optimum length and there is no time dependence. Time-lapse Movies S1–S3 correspond, respectively, to Fig. 2 *A*, *C*, and *D*.

Swimmers Exhibiting Negative Autochemotaxis

While a droplet swimmer moves through the solution, it will leave a trail of filled micelles behind, such that the fraction of empty micelles in the trail decreases. Because the swimmers are sensitive to the density of empty micelles, they will therefore avoid their own trail, i.e., exhibit negative autochemotaxis.

This is shown qualitatively in Fig. 3. Fig. 3*A* shows a 5CB droplet swimming in a surfactant solution of high concentration (25 wt% TTAB) and high temperature (37 °C), resulting in a high solubilization rate. A trail of oil-filled micelles, dispersing over time in the wake of the droplet, can be inferred from variations in the refractive index in the aqueous phase.

In Fig. 3*B* we have plotted three trajectories of isotropic 5CB swimmers ($T = 37°$C, 7.5 wt% TTAB) interacting in a Hele–Shaw cell, with markers on the trajectories labeling the time since the start of observation. The first swimmer, marked 1, moves in an unperturbed manner, but swimmer 2 is repelled from swimmer 1's trail, even though swimmer 1 passed 20 s earlier. Swimmer 3 approaches swimmer 2's trajectory more closely, 5 s after 2's passage, but is turned away sharply. This is consistent with a steep gradient in filled micelles in the not yet strongly dispersed trail directly behind a swimmer, leading to a stronger and more short-ranged chemotactic repulsion than in the interaction between swimmers 1 and 2. Note that due to the quasi-2D geometry of the cell, hydrodynamic interactions are suppressed for droplet distances exceeding the cell height of 50–55 μm.

Branch Choice by Autochemotactic Signaling

Autochemotactic processes are generally treated considering the following aspects: the secretion and decay of the chemical constituting the trail, the diffusion of the trail, and the interaction of the swimmer with the self-generated chemical gradient. Appropriate simulations on autochemotaxis (26, 28) have been conducted using parameters extracted from experimental studies (24, 37). Inspired by Ambravaneswaran et al. (46), we have designed a microfluidic experiment to study autochemotactic processes quantitatively by having multiple swimmers consecutively pass a series of bifurcations in a channel.

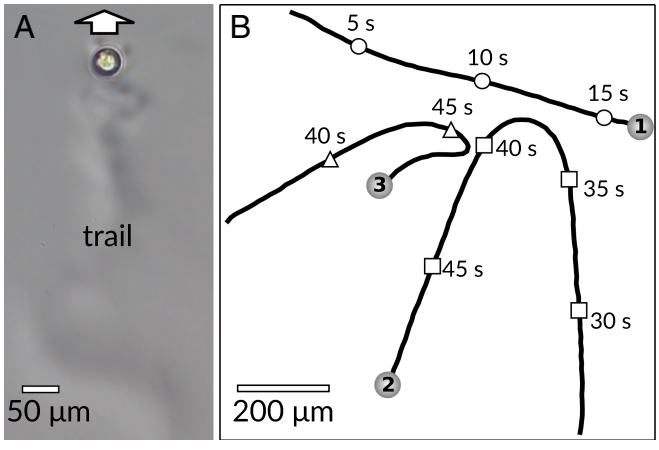

Fig. 3. (*A*) A droplet swimmer leaves a trail that can be seen under phase-contrast microscopy from the slightly different refractive index. (*B*) Free swimmers avoiding each other's trails. Sphere drawings (to scale) mark the trajectory end points, timing marks on trajectories' time points in the experiment (Movies S4 and S5).

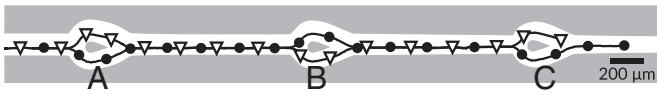

Fig. 4. Swimmers moving through bifurcating channels choose alternating branches. Two trajectories of different swimmers are plotted in lines and marked by solid circles (first) and open triangles (second) in the order of passage [Movie S6 and Fig. S1 (cell design)].

The autochemotaxis problem is reduced to a simple measure of correlated binary branch choices, resulting in a high statistical yield. We have fitted such correlation data with an analytical model balancing a gradient force against a stochastic noise term. In the model, we assume that the coupling between the gradient in filled micelles and the repulsive chemotactic force is linear and that micellar diffusion determines the gradient evolution over time.

We begin with an example experimental run: In Fig. 4, we have drawn a channel pattern with three bifurcations *A*, *B*, and *C* (white mask) and overlaid it with two selected trajectories for 5CB/BPD swimmers. The channel connects an entrance with a large exit reservoir; symmetric bifurcations are generated by a series of pillars, which are tear shaped with the pointed end facing the exit reservoir to keep the swimmers from turning back around the pillar. This pinch-off design is quite efficient: in our experiments, 75% of swimmer interactions with the pillar contained only one passage through a single branch. Note that there is no overall flow or surfactant gradient between the entrance and exit of the channel. The trajectories are marked by a solid circle (swimmer 1) and an open triangle (swimmer 2), in the order of passage. Swimmer 2 enters the channel approximately 20 s after swimmer 1. The two swimmers are anticorrelated in their choice at all bifurcations.

The trail secretion of a solubilizing droplet (β molecules per swimmer per second) can be established from the solubilization rate—i.e., the time-dependent droplet size. Contrary to most biological autochemotactic systems, there is no decay of the secretion products. Because the width and height of the channel, $w = 100$ μm and $h = 110$ μm, are of the order of the initial swimmer diameter $2r = 100$ μm, we assume the filled-micelle density to be constant over the channel cross-section. We can therefore map our model of trail diffusion and autochemotactic branch choice to a one-dimensional (1D) problem along the channel midline around the pillar. The number density of the solubilized oil molecules in the trail directly behind the swimmers is $c_0 = \beta/(vwh)$, with the speed of the swimmers v and the channel width w extracted from the experiment. We approximate the initial secretion profile $c(x)$ in the channel by a 1D step function. The average duration of a channel passage is ca. 15 s and we set the time origin $t = 0$ to the instant when the first swimmer leaves the bifurcation at $x = -l$. Because the step function approximation is not valid for short times and we expect pressure equilibration flows around the pillar when the first droplet leaves, we use only events for data fitting where the second droplet enters the junction more than 20 s after the first one left it ($\Delta t > 20$ s).

To model the diffusion of the oil-filled micelles, we approximate the bifurcation by a circular pillar of radius $R = 2l/\pi$ and use a polar coordinate at fixed radius $x = R \cdot \theta$ with the angle $\theta = 0$ at the top of the pillar, progressing counterclockwise, such that the entrance bifurcation is at $x = l$ (Fig. 5*A*). Without loss of generality, we assume that the swimmer enters the bifurcation from the left at $x = l$ and chooses the top branch.

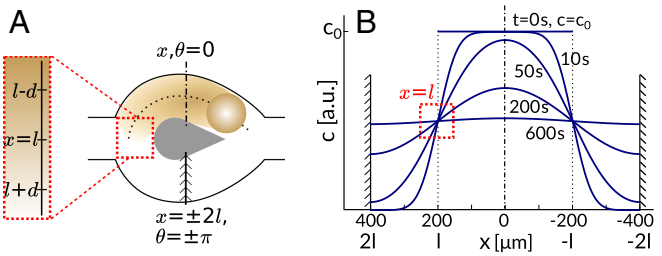

Fig. 5. (*A*) Schematic drawing of a bifurcation. The trail of a swimmer fills the top branch and diffuses into the bottom branch around the pillar. The bifurcation is mapped to a fixed radius polar coordinate $x = (2l/\pi) \cdot \theta$ with the origin at the top of the bifurcation and $x = l$ at its entrance. (*B*) Trail dispersion, characterized by the concentration profile of micellar-solubilized oil molecules *c*, approximated by 1D diffusion from a step function between reflecting boundaries, with calculated profiles for times between 0 s and 600 s. Red dotted rectangle marks the gradient at $x = l$.

In our circular pillar approximation, the diffusion problem is symmetric around $x = 0$, and we neglect diffusion into the main channel at $x = \pm l$. The gradient evolution at $x = l$ can be mapped onto the problem of 1D diffusion between two reflecting or periodic boundaries at $x = \pm 2l$ (Fig. 5*B*). The concentration profile in the region $-2l \le x \le 2l$ evolving over time from a step function $c(-l \le x \le l) = c_0$ is (47)

$$c(x,t) = \frac{c_0}{2} \sum_{n=-\infty}^{\infty} \left(\mathrm{erf} \frac{(4n+1)l - x}{\sqrt{4D_f t}} - \mathrm{erf} \frac{(4n-1)l - x}{\sqrt{4D_f t}} \right), \quad [1]$$

where D_f denotes the diffusion coefficient of the filled micelles, which are the carriers of the solubilized oil. We provide a full derivation in the *Supporting Information*.

Using parameters appropriate to our experimental system [$l \approx 200$ μm, $D_f \approx 100$ μm$^2 \cdot$s^{-1} (48)], we calculate and plot examples of concentration profiles at different times in Fig. 5*B*. We expect the anticorrelation between the choices of two consecutive swimmers to decay in time, depending on the decrease of the gradient at $x = l$. In the long time limit, after the environment in the two branches becomes homogeneous again, the choice of a swimmer between the two branches should be completely random, i.e., independent of the choice of the previous swimmer.

The swimmers make their choice at the entrance $x = l$ under both the gradient force and the stochastic force. In all experiments, we did not observe swimmers reversing direction once past the bifurcation. This indicates that the choice is made within a small region $x \in [l - d, l + d]$, as sketched in Fig. 5*A*, with d on the order of the droplet diameter or channel width, and on a timescale τ much shorter than the timescale t of the trail dispersion. Hence, the motion of the swimmer $x(\tau)$ during the decision process can be approximated as a 1D Brownian motion under a constant gradient force between two absorbing boundaries at $l \pm d$, described by the following overdamped Langevin equation:

$$\left. \frac{dx}{d\tau} \right|_{x=l} = \kappa \partial_x c + \sqrt{2D}\Gamma(\tau). \quad [2]$$

Here, κ is a linear coefficient quantifying the sensitivity to the chemorepellent gradient $\partial_x c$. Because the chemorepellent is self-produced, κ corresponds to the autochemotactic feedback strength used in the literature (26–30). Note that κ is not identical to the chemotactic strength as applicable to the maze experiments, which is based on a gradient in empty micelles. $\Gamma(\tau)$ is a normalized Gaussian noise term with $\langle \Gamma(\tau) \rangle = 0$, $\langle \Gamma(\tau), \Gamma(\tau + \Delta\tau) \rangle = \delta(\Delta\tau)$. The velocity of the active swimmer is not included in Eq. **2**, as the branch choice direction is orthogonal to the incoming swimmer. D denotes the diffusion coefficient of a passive swimmer and is presumably larger than the Stokes–Einstein value of $k_B T/6\pi\eta r$, because the micellar solubilization process provides an additional source of stochastic noise.

The position of the swimmer $x(\tau)$ can be written as

$$x(\tau) - l = \kappa \partial_x c\, \tau + \sqrt{2D} B^{\circ}(\tau), \quad [3]$$

where $B^{\circ}(\tau)$ is a standard Brownian motion process and $x(0) = l$.

The probability $\mathcal{P}$ of anticorrelated branch choices between two consecutive swimmers is then the probability that the biased Brownian motion process $x(\tau)$ reaches $l + d$ before $l - d$ (49):

$$\mathcal{P} = \frac{1 - \exp(-2\xi)}{\exp(2\xi) - \exp(-2\xi)}, \quad \xi = -\frac{\kappa \cdot d}{2D} \partial_x c. \quad [4]$$

In our data analysis, we record events of correlated branch choices between consecutive swimmers as $\mathcal{C} = 1$ and anticorrelated choices as $\mathcal{C} = -1$. If the interaction of a swimmer and a pillar contains several passages, i.e., the swimmer orbits the pillar, we consider only the last passage of the preceding swimmer and the first passage of the following swimmer. To study the time-dependent decay of the (anti)correlation, we bin the experimental result according to the time interval Δt between the preceding swimmer leaving the bifurcation and the following swimmer entering it. Using Eq. **4** with a concentration gradient $\partial_x c$ at $x = l$, $t = \Delta t$, the average correlation between the choices of consecutive swimmers is

$$\langle \mathcal{C} \rangle = -1 \cdot \mathcal{P} + 1 \cdot (1 - \mathcal{P}) = \tanh(\xi(\Delta t)). \quad [5]$$

The statistical result for $\langle \mathcal{C} \rangle$ from a series of branch-choosing experiments is shown in Fig. 6. Because some microfluidic bifurcations can be biased due to fabrication errors, we accepted only results from bifurcations where the overall preference for a single branch was less than 75%. The bias-corrected dataset contains 4,160 correlation events, omitting 283 rejected events. The data are binned by the time interval Δt; the average correlation $\langle \mathcal{C} \rangle$ of each bin is plotted vs. the corresponding average Δt (blue bars). To account for the steep correlation decay for short times and decreasing statistics for long times, we use a constant number of events (100 swimmer pairs) per bin, resulting in an increasing range of time intervals, indicated by the bar width.

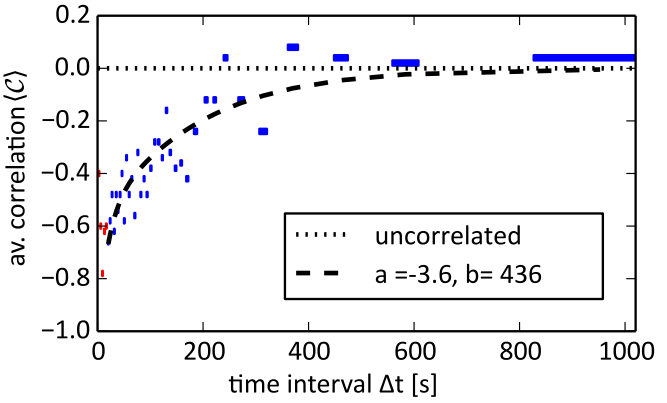

Fig. 6. Correlation $\langle \mathcal{C} \rangle$ between branch choices of consecutive swimmers vs. the time interval Δt between passages. Data were binned by Δt using 100 events per bin and then averaged (the corresponding Δt range is marked by the bar width). $\langle \mathcal{C} \rangle$ decorrelates with increasing Δt, with the limits of $\langle \mathcal{C} \rangle \in [-1, 0]$ for perfect anticorrelation (−1) and no correlation (0). The parameters $a = -3.6 \pm 0.2$ and $b = (4.3 \pm 1.2) \times 10^2$ s for the fitted $\langle \mathcal{C} \rangle = \tanh(\xi)$ were derived by fitting ξ using Eqs. **5**–**7**. Correlation data for $\Delta t < 10$ s (red bars) were omitted from the fitting to rule out hydrodynamic drag effects. Supplementary data on the effects of TTAB concentration and channel geometry are provided in Figs. S2 and S3.

When Δt is small, the choices of swimmers show a clear anticorrelation up to -0.8; i.e., 90% of the following swimmers choose the branch that the preceding swimmer did not pass. As Δt increases, this average anticorrelation decreases to values close to zero; i.e., swimmers enter branches randomly and independent of the preceding swimmer.

With Eq. **5**, ξ can be easily calculated from the anticorrelation data. We truncate the concentration profile from Eq. **1** to the $n = 0, \pm 1$ terms and fit ξ with

$$\xi = -\frac{a}{\sqrt{t}}(2\exp(-b/t) - 1 - 2\exp(-4b/t) + \exp(-9b/t)), \quad [6]$$

with two parameters, a prefactor a and a time constant b:

$$a = \frac{\kappa}{D} \cdot \frac{\beta\, d}{4vwh\sqrt{\pi D_\mathrm{f}}}, \quad b = \frac{l^2}{D_\mathrm{f}}. \quad [7]$$

The corresponding function for the average correlation $\langle \mathcal{C} \rangle$ is then plotted in Fig. 6 as black dashes.

With $b \approx 436$ s from fitting the experimental data and $l \approx 200$ μm, we calculated $D_\mathrm{f} \approx 92\ \mu\mathrm{m}^2 \cdot \mathrm{s}^{-1}$, which agrees with calculated and literature values ($D_\mathrm{f} \approx 100\ \mu\mathrm{m}^2 \cdot \mathrm{s}^{-1}$) (48). In our expression for a in Eq. **7**, all quantities except the autochemotactic coupling strength κ and the droplet diffusion coefficient D can be measured or calculated independently. We can therefore use a as a direct measure of the strength of chemotactic vs. stochastic forces, κ/D.

Conclusion and Summary

We studied a system of self-propelled droplets that exhibits chemotaxis comparable to that of biological systems. The motion of the oil-in-water droplets is driven by a Marangoni flow, which is caused by a self-sustained interfacial tension gradient during the solubilization of the droplet in a micellar surfactant solution. In a homogeneous solution, the swimmers show no directional preference, whereas they move up surfactant gradients, i.e., gradients in empty micelles, whose effect we have used to guide them through microfluidic mazes.

A related effect is trail avoidance by negative autochemotaxis, due to gradients of oil-filled micelles in the wake of a droplet. We have studied this effect quantitatively, observing anticorrelated branch choices between consecutive droplets in microfluidic channel bifurcations. We could model the time-dependent correlation decay analytically, assuming a force on the droplets proportional to the local empty micelle gradient.

Fitting our data yielded two system parameters: a time constant b depending on the micellar diffusion timescale and a linear prefactor a, containing the secretion rate β and the strength of (auto)chemotaxis κ over stochastic force D. In biological systems, where various physical effects and bioprocesses are intertwined, these parameters are often difficult to measure independently. Microfluidic assays as presented above can provide reproducibly quantitative experimental data for statistics and comparative studies. In our droplet swimmer system, we will use insights from this study to predict and control autochemotactic effects in more complicated geometries and to compare the swimmer dynamics with theoretical models (26–30).

Materials and Methods

Chemicals. We obtain 5CB, BPD, TTAB, and Nile Red from commercial suppliers (Synthon Chemicals and Sigma-Aldrich) and use them as is.

Microfluidic Devices. We fabricate microfluidic devices using standard soft lithography procedures: We create photomasks in a 2D AutoCad application and have them printed as a high-resolution emulsion film by an external company (128,000 dots per inch; JD Photo-Tools). A Si wafer (Wafer World Inc.) is spin coated with a negative photoresist (SU-8; Micro Resist Technology) in a clean room environment. UV light exposure through a photomask and subsequent chemical development produce a master wafer containing the microstructures.

We then use the master wafer in a polymer molding step to cast the microstructure into PDMS (polydimethylsiloxane; Sylgard 184; Dow Corning). After degassing and heat curing at 75 °C for 2 h, we peel the PDMS replica off the wafer, cut it into single pieces, and punch in fluid inlets and outlets. We then seal the molded PDMS blocks from below by glass slides. Covalent bonding between PDMS and glass is achieved by pretreating all surfaces in an air plasma (Pico P100-8; Diener Electronic GmbH + Co. KG) for 30 s.

We produce droplets in standard flow-focusing microfluidic devices, mounting syringes (Braun) on a precision microfluidic pump (NEM-B101-02B; Cetoni GmbH) and connecting them to the inlets and outlets with Teflon tubing (39241; Novodirect GmbH). To create oil-in-water emulsions, we first activate the originally hydrophobic PDMS surfaces by a 1:1 volumetric mixture of H_2O_2/HCl, then fill the channels with a silanization solution [$(C_2H_2O)_n$ $C_7H_{18}O_4Si$] for 30 min, and finally rinse them with milli-Q water.

During experiments, we introduce a concentrated droplet stock solution into microfluidic devices, using standard pipettes.

Image Recording and Analysis. We record swimmers (still images and movies) on an Olympus IX-73 optical microscope connected to a commercial digital camera (Canon EOS 600D) at four frames per second. Images are processed (swimmer tracking and trajectory analysis) using software written in-house in Python/openCV.

ACKNOWLEDGMENTS. Discussions with R. Breier, F. Schwarzendahl, C. Bahr, and S. Herminghaus are gratefully acknowledged. C.J. is supported by the Federal Ministry of Education and Research/Max Planck Society's "MaxSynBio" consortium and C.K. by the German Research Foundation (Priority Program 1726).

1. Madigan MT, Martinko JM, eds (2006) Bacterial cell surface structures. *Brock Biology of Microorganisms* (Prentice Hall, Upper Saddle River, NJ).
2. Adler J (1966) Chemotaxis in bacteria. *Science* 153:708–716.
3. Hazelbauer GL (2012) Bacterial chemotaxis: The early years of molecular studies. *Annu Rev Microbiol* 66:285–303.
4. Čejková J, et al. (2016) Chemotaxis and chemokinesis of living and non-living objects. *Advances in Unconventional Computing*, ed Adamatzky A (Springer, Basel, Switzerland), pp 245–260.
5. Wadhams GH, Armitage JP (2004) Making sense of it all: Bacterial chemotaxis. *Nat Rev Mol Cell Biol* 5:1024–1037.
6. Bonner JT, Savage L (1947) Evidence for the formation of cell aggregates by chemotaxis in the development of the slime mold Dictyostelium discoideum. *J Exp Zool* 106:1–26.
7. Zhao K, et al. (2013) Psl trails guide exploration and microcolony formation in Pseudomonas aeruginosa biofilms. *Nature* 497:388–391.
8. Drescher K, Goldstein RE, Tuval I (2010) Fidelity of adaptive phototaxis. *Proc Natl Acad Sci USA* 107:11171–11176.
9. Couzin ID (2009) Collective cognition in animal groups. *Trends Cognit Sci* 13:36–43.
10. Jackson DE, Martin SJ, Holcombe M, Ratnieks FL (2006) Longevity and detection of persistent foraging trails in Pharaoh's ants, Monomorium pharaonis (L.). *Anim Behav* 71:351–359.
11. Lagzi I, Soh S, Wesson PJ, Browne KP, Grzybowski BA (2010) Maze solving by chemotactic droplets. *J Am Chem Soc* 132:1198–1199.
12. Čejková J, Novák M, Štěpánek F, Hanczyc MM (2014) Dynamics of chemotactic droplets in salt concentration gradients. *Langmuir* 30:11937–11944.
13. Abecassis B, Cottin-Bizonne C, Ybert C, Ajdari A, Bocquet L (2008) Boosting migration of large particles by solute contrasts. *Nature materials* 7:785–789.
14. Dreyfus R, et al. (2005) Microscopic artificial swimmers. *Nature* 437:862–865.
15. Maass CC, Krüger C, Herminghaus S, Bahr C (2016) Swimming droplets. *Annu Rev Condens Matter Phys* 7:171–193.
16. Toyota T, Maru N, Hanczyc MM, Ikegami T, Sugawara T (2009) Self-propelled oil droplets consuming "fuel" surfactant. *J Am Chem Soc* 131:5012–5013.
17. Izri Z, Van Der Linden MN, Michelin S, Dauchot O (2014) Self-propulsion of pure water droplets by spontaneous Marangoni-stress-driven motion. *Phys Rev Lett* 113:248302.
18. Ismagilov RF, Schwartz A, Bowden N, Whitesides GM (2002) Autonomous movement and self-assembly. *Angew Chem Int Ed* 41:652–654.
19. Golestanian R, Liverpool TB, Ajdari A (2005) Propulsion of a molecular machine by asymmetric distribution of reaction products. *Phys Rev Lett* 94:220801.
20. Howse JR, et al. (2007) Self-motile colloidal particles: From directed propulsion to random walk. *Phys Rev Lett* 99:048102.
21. Buttinoni I, Volpe G, Kümmel F, Volpe G, Bechinger C (2012) Active Brownian motion tunable by light. *J Phys Condens Matter* 24:284129.

22. Lozano C, Ten Hagen B, Löwen H, Bechinger C (2016) Phototaxis of synthetic microswimmers in optical landscapes. *Nat Commun* 7:12828.
23. Budrene E, Berg H (1995) Dynamics of formation of symmetrical patterns by chemotactic bacteria. *Nature* 376:49–53.
24. Brenner MP, Levitov LS, Budrene EO (1998) Physical mechanisms for chemotactic pattern formation by bacteria. *Biophys J* 74:1677–1693.
25. Yashin VV, Kolmakov GV, Shum H, Balazs AC (2015) Designing synthetic microcapsules that undergo biomimetic communication and autonomous motion. *Langmuir* 31:11951–11963.
26. Tsori Y, De Gennes PG (2004) Self-trapping of a single bacterium in its own chemoattractant. *Europhys Lett* 66:599–602.
27. Grima R (2005) Strong-coupling dynamics of a multicellular chemotactic system. *Phys Rev Lett* 95:128103.
28. Sengupta A, van Teeffelen S, Löwen H (2009) Dynamics of a microorganism moving by chemotaxis in its own secretion. *Phys Rev E* 80:031122.
29. Taktikos J, Zaburdaev V, Stark H (2011) Modeling a self-propelled autochemotactic walker. *Phys Rev E* 84:041924.
30. Kranz WT, Gelimson A, Zhao K, Wong GCL, Golestanian R (2016) Effective dynamics of microorganisms that interact with their own trail. *Phys Rev Lett* 117:038101.
31. Theurkauff I, Cottin-Bizonne C, Palacci J, Ybert C, Bocquet L (2012) Dynamic clustering in active colloidal suspensions with chemical signaling. *Phys Rev Lett* 108:268303.
32. Pohl O, Stark H (2014) Dynamic clustering and chemotactic collapse of self-phoretic active particles. *Phys Rev Lett* 112:238303.
33. Liebchen B, Marenduzzo D, Pagonabarraga I, Cates ME (2015) Clustering and pattern formation in chemorepulsive active colloids. *Phys Rev Lett* 115:258301.
34. Peddireddy K, Kumar P, Thutupalli S, Herminghaus S, Bahr C (2012) Solubilization of thermotropic liquid crystal compounds in aqueous surfactant solutions. *Langmuir* 28:12426–12431.
35. Herminghaus S, et al. (2014) Interfacial mechanisms in active emulsions. *Soft Matter* 10:7008–7022.
36. Berg HC, Turner L (1990) Chemotaxis of bacteria in glass capillary arrays. Escherichia coli, motility, microchannel plate, and light scattering. *Biophys J* 58:919–930.
37. Van Haastert PJ, Postma M (2007) Biased random walk by stochastic fluctuations of chemoattractant-receptor interactions at the lower limit of detection. *Biophys J* 93:1787–1796.
38. Jeon NL, et al. (2002) Neutrophil chemotaxis in linear and complex gradients of interleukin-8 formed in a microfabricated device. *Nat Biotechnol* 20:826–830.
39. Irimia D, et al. (2006) Microfluidic system for measuring neutrophil migratory responses to fast switches of chemical gradients. *Lab Chip* 6:191–198.
40. Mao H, Cremer PS, Manson MD (2003) A sensitive, versatile microfluidic assay for bacterial chemotaxis. *Proc Natl Acad Sci USA* 100:5449–5454.
41. Song L, et al. (2006) Dictyostelium discoideum chemotaxis: Threshold for directed motion. *Eur Jo Cell Biol* 85:981–989.
42. Amselem G, Theves M, Bae A, Beta C, Bodenschatz E (2012) Control parameter description of eukaryotic chemotaxis. *Phys Rev Lett* 109:108103.
43. Amselem G, Theves M, Bae A, Bodenschatz E, Beta C (2012) A stochastic description of Dictyostelium chemotaxis. *PLoS One* 7:e37213.
44. Krüger C, Klös G, Bahr C, Maass CC (2016) Curling liquid crystal microswimmers: A cascade of spontaneous symmetry breaking. *Phys Rev Lett* 117:048003.
45. Kim TH, Jung SH, Cho KH (2008) Investigations into the design principles in the chemotactic behavior of Escherichia coli. *Biosystems* 91:171–182.
46. Ambravaneswaran V, Wong IY, Aranyosi AJ, Toner M, Irimia D (2010) Directional decisions during neutrophil chemotaxis inside bifurcating channels. *Integr Biol* 2:639–647.
47. Crank J (1975) Methods of solution when the diffusion coefficient is constant. *The Mathematics of Diffusion* (Oxford Univ Press, Oxford, UK), pp 13–24.
48. Candau S, Hirsch E, Zana R (1984) New aspects of the behaviour of alkyltrimethylammonium bromide micelles: Light scattering and viscosimetric studies. *J Phys* 45:1263–1270.
49. Pinsky MA, Karlin S (2013) Brownian motion and related processes. *An Introduction to Stochastic Modeling* (Elsevier, Singapore), 4th Ed, 419–421.